# Moving Target Detection on SAR Images

**Hélène Oriot**
ONERA - The French Aerospace Lab
F-91761 Palaiseau
France

helene.oriot@onera.fr

## *ABSTRACT*

*Synthetic aperture radar (SAR) is a well known technique for generating high-resolution images stationary scenes but it is not adapted to imaging moving targets as the movement of a target induces both a delocalization and a defocusing effect in a SAR image. The aim of this paper is to analyse the signatures of moving targets in SAR images and to present techniques to detect them, from one single image to multiple SAR images.*

## 1.0 INTRODUCTION

The problem of detection and localisation of moving targets using airborne radar data has been studied for a long time and solutions have been implemented:

- The MTI (Moving target indicator) technique is adapted to high velocity targets and is based on the processing of multi temporal data. The target is detected when its Doppler frequency is out of the Doppler spread of the clutter environment (exo-clutter targets).

- STAP (Space Time Adaptive processor) techniques [1], are based on the coherent processing of train of pulses received on multiple antennas. These techniques aim at lowering the ground clutter response to enhance moving target response even if the Doppler of the moving target remains within the Doppler spread of the clutter environment (endo-clutter targets).

The waveform used for both MTI and STAP is optimised: generally the transmitted bandwidth is narrow and the PRF (Pulse Repetition Frequency) is high in order to increase the velocity range of non-ambiguous targets and to enlarge the exo-clutter zone. Furthermore, the antenna tends to have a very narrow beam in order to diminish the endo-clutter zone, the burst interval is short (of the order of 50 ms for X band systems) and the antenna can be steered from aft to front in order to survey large areas. With these techniques, only targets with non-zero radial velocity can be detected and localise with an error which depends on (1) the radar configuration, (2) target RCS and (3) target velocity. Usually this uncertainty is of the order of a fraction of the antenna pattern. The minimum detectable radial velocity also depends on the radar configuration and on the target RCS [1]. After detection, tracking is performed in order to retrieve target tracks and the complete cinematic vector of targets.

On the other side, SAR imaging consists in imaging a ground area from a moving platform (airborne or spaceborne most of the time) and on using the movement of the carrier to image non moving objects with a high resolution [2] which enable target recognition [3]. Here also, the radar waveform is optimised: the transmitted bandwidth is wide in order to obtain good range resolution, the PRF is generally low in order to decrease range-ambiguities and the antenna pattern tends to be broader than for MTI modes, especially for stripmap mode since in this mode the achievable azimuth resolution is lower bounded by half the antenna size.

These two modes (MTI/STAP and SAR) are closely related: Both techniques process coherently train of pulses but, for MTI application, these bursts are quite short whereas SAR processing requires much longer bursts. MTI/STAP uses multiple receiver antennas whereas regular SAR uses only one receiver antenna but related techniques known as ATI compare two or more SAR images acquired with antenna placed along-track. Operationally, these two modes, MTI/STAP and SAR are complementary-, MTI/STAP would detect a moving target and the second is fitted to recognise non -moving targets.

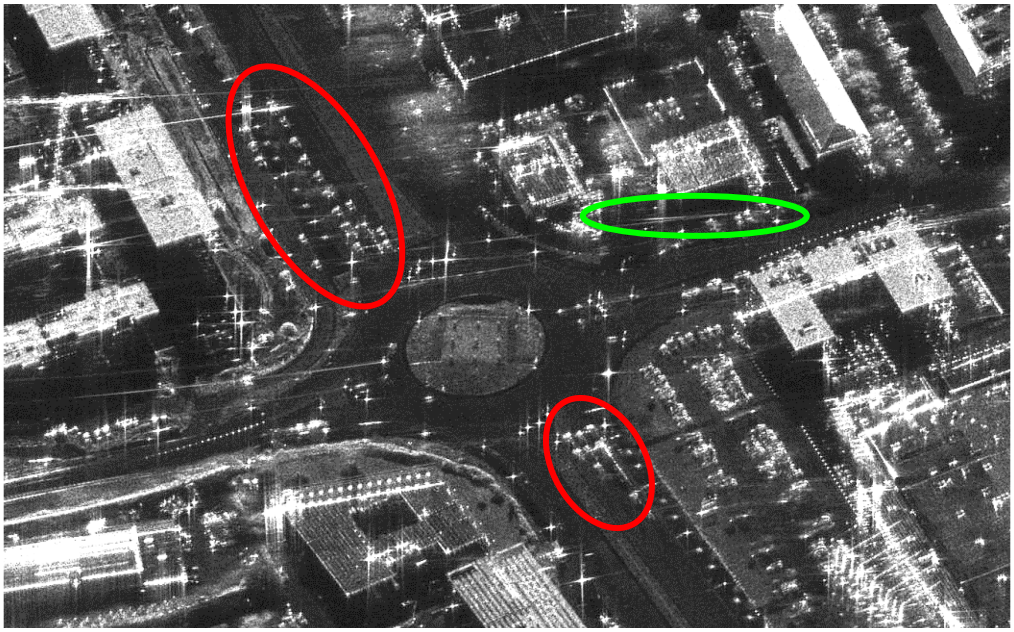

**Figure 1: High resolution image with stationary cars stopped at red light (circled in red) and moving cars signatures (circled in green).**

In order to make use of both techniques efficiently two different strategies are commonly studied:

- The first one consists in developing radar with changing mode capabilities: MTI/STAP and SAR are implemented together and are used alternatively.
- The second one consists in examining the potentiality of the SAR mode for moving target detection.

In this context, the aim of this paper is to present the state of the art of moving target detection using SAR imaging. In the following section we will present the notations used in this paper. Section 3 will be dedicated to the presentation of SAR processing techniques and the effect of moving targets on SAR images. Then, the problematic of moving target detection will be addressed in the case of one SAR image (section #4), two SAR images (section #5) and multiple SAR images (section #6).

## 2.0 NOTATIONS

The following notations will be used through this paper:

- $s_i(R)$ is the raw signal located at range $R$, after range compression for pulse $\#i$
- $P$ is the imaged point on the ground
- Si with i=1...T are the position of the sensor during the integration time $T$

- PRF (Pulse Repetition Frequency) is the inverse of the time interval between the transmission of two consecutive pulses
- **Vs** is the sensor velocity vector, Vs is the norm of this vector
- **v** and **a** are a target velocity and acceleration vectors, v and a are the norms of these vectors, $v_r$ is the radial velocity of the target, $v_a$ is the along track velocity of the target;
- θ is defined so that π/2- θ is the angle between the radar velocity vector $\mathbf{V_s}$ and the line of sight.
- $x_{i,j}$ is the complex radiometry of pixel $(i,j)$ of interest The *i*-or *y* axis- corresponds to the along track direction, the *j* -or *x* axis-, to the corresponds range direction.
- x* stands for the complex conjugate of x
- λ is the wavelength associated with the central frequency of the emitted wave.

# 3.0 EFFECTS OF A MOVING TARGET ON SAR IMAGES

## 3.1 SAR processing principle

At a given time *t*, the radar transmits a wave with a given azimuthal footprint. This footprint depends on the kind of array implemented and is inversely proportional to the antenna azimuthal length (Figure 2, left). For real aperture radar, the along-track instantaneous resolution of the output image is therefore related to the width of the antenna array. The SAR technique uses the displacement of the sensor along the trajectory of the platform to simulate a "synthetic antenna" with a longer length leading to a higher azimuth resolution (Figure 2, right). In doing so, SAR imaging uses signals acquired at different times to form a single image.

Mathematically, the signals are summed coherently after having being rephased.

$$S_p = \sum_{i=1}^{M} s_i(R_i) e^{j4\pi\frac{R_i}{\lambda}} \text{ with } R_i = |\mathbf{S_i P}| \quad (1)$$

The geometrical interpretation of SAR focusing is the following (see 0): For each acquisition time $t_i$ ($t_1<t_i<t_M$), let's $R_i$ be the distance between P and $S_i$. All the points located at the exact same distance $R_i$ from the sensor $S_i$ located within the real antenna footprint are part of the signal received by the radar at time $t_i$. By adding coherently the different rephased signals, the SAR processing enhances the backscattering of point P which is the intersection of the different circles, centered in $S_i$ at range $R_i$. Note that the most important part is the rephasing part that compensates the phase variations induced by $R_i$ ; This compensation has to be done with an accuracy of a fraction of the wavelength.

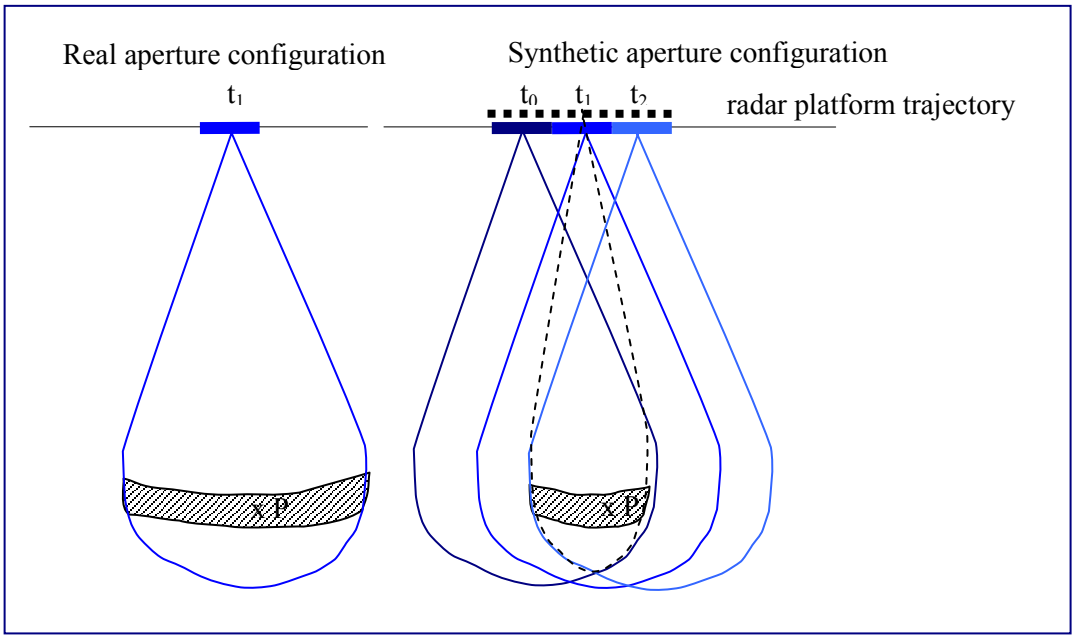


**Figure 2: Geometrical configuration of SAR imaging. Left image: real aperture configuration. The physical antenna is represented as a blue segment and its antenna pattern is indicated in blue. The dashed area corresponds to the azimuthal real antenna resolution cell. Right figure: the different positions of the real antenna are represented in blue, and the resulting synthetic antenna pattern and resolution cell appears in the dotted lines.**

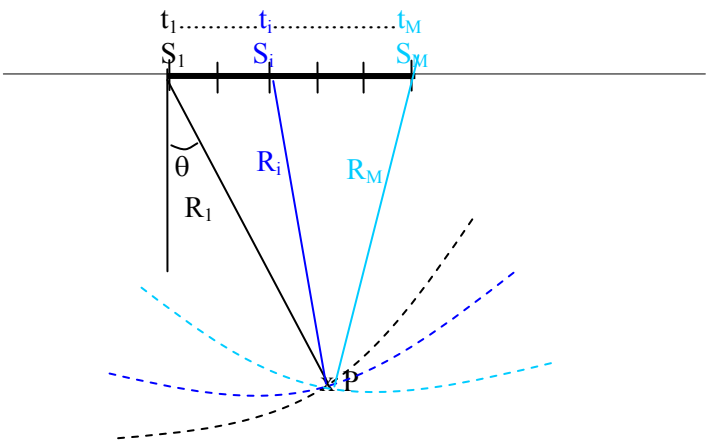


**Figure 3: Geometrical interpretation of SAR focusing.**

It is interesting to interpret equation (1) from a frequency point of view:

Let's develop $R_i$. Let's $S_1$ be the reference position of the sensor and $R_1$ the distance between the sensor at position $S_1$ and P. θ is defined so that $\pi/2 - \theta$ is the angle between the radar velocity vector $\mathbf{V_s}$ and $\mathbf{S_1P}$.

$$R_i = S_i P = \left|\mathbf{S_1P - S_1S_i}\right| = \left|\mathbf{S_1P - V_s}t\right| = R_1\sqrt{1 - \frac{2\mathbf{S_1P.S_1S_i}}{R_1^2} + \frac{V_s^2}{R_1^2}t^2} \quad \text{with } t=t_i-t_0$$

The Taylor's expansion in t of $R_i$. up to the second order gives:

$$R_i \approx R_1\left(1 - \frac{V_s \sin\theta}{R_1}t + \frac{V_S^2 \cos^2\theta}{2R_1^2}t^2\right) \tag{2}$$

It corresponds to the Doppler frequency:

$$F_d = -\frac{2}{\lambda}\frac{dR}{dt} = \frac{2V_s \sin\theta}{\lambda} \tag{3}$$

And a Doppler frequency modulation rate (FM):

$$FM = -\frac{2}{\lambda}\frac{d^2R}{dt^2} = \frac{2V_S^2 \cos^2\theta}{\lambda R_1} \tag{4}$$

Up to the second order, the Doppler frequency of a stationary point varies linearly with long time. Therefore, it is theoretically possible to focus the image in azimuth using a match filter and the output resolution in the azimuth direction is given by the formula:

$$res_{az} = \frac{V_S}{FM.T} = \frac{\lambda R_1}{2V_s T\cos^2\theta} = \frac{\lambda R_1}{2L\cos^2\theta} \tag{5}$$

This resolution corresponds to the integration of signals between squint angle θ and squint angle θ+δθ with

$$\delta\theta = \frac{L\cos\theta}{R_1}. \tag{6}$$

Equation (3) shows that, for narrow band signals, the doppler frequency is proportional to the squint angle. Therefore, the clutter doppler spread is related to the two extreme squint angles of the antenna footprint as drawn on 0, left. This domain is called the endo-clutter domain.

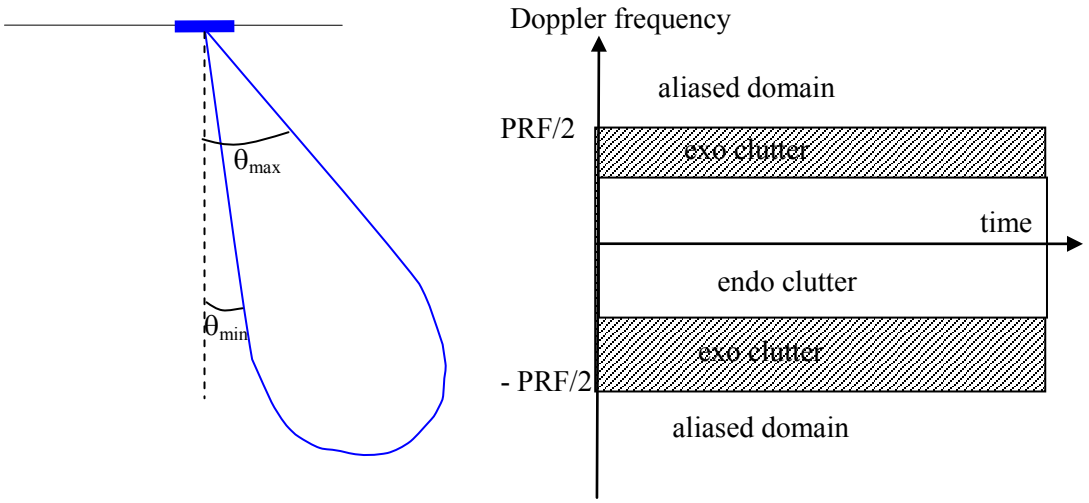


**Figure 4: Representation of the clutter doppler spread in term of squint angles, versus Doppler frequency representation of a fixed beam acquisition geometry.**

Furthermore, the PRF of the system gives a boundary limit of the Doppler domain that is recorded: [-PRF/2 PRF/2]. Doppler frequencies outside this range are wrapped into this interval. The interval located between the clutter domain and the domain defined by the PRF is called the exo-clutter domain since no response from the ground is expected.

SAR processing may be done in various ways. Generally, for fixed beam geometry, SAR processing is done for a given mean squint angle. In operational systems, the doppler processed interval is close to the clutter doppler domain in order to optimise the signal to noise ratio of the system. It is also possible to separate the doppler clutter domain in sub-bands and processed each interval, resulting in a set of images centered on different Doppler frequencies. Each azimuth of these stripmap images corresponds to integration over a different portion of the sensor trajectory, thus each azimuth of the image corresponds to at a different time of acquisition. This geometry is illustrated in 0 left side. Another way of processing the radar raw data is to consider one single portion of trajectory and to compute an image with each azimuth line corresponding to a different squint angle (0 right). This is a focused version of the well known Doppler Beam Sharpening (DBS) technique. Example of such an image is presented in 0. This kind of images will be named FDBS (Focused Doppler Beam Sharpening) in the following.

Several techniques have been developed to efficiently implement SAR processing.

- First backprojection algorithms [4] implemented in the time domain correspond to the direct implementation of equation (1). They are adapted to airborne data since they can cope with non linear motion of platform velocity. They use the hypothesis of narrow band radar since the phase correction is performed for the center frequency.

- Range-Doppler Algorithm (RDA), Chirp Scaling Algorithm (CSA) and ω-k algorithms are implemented in the frequency domain [2] and can also be adapted to airborne data [5].

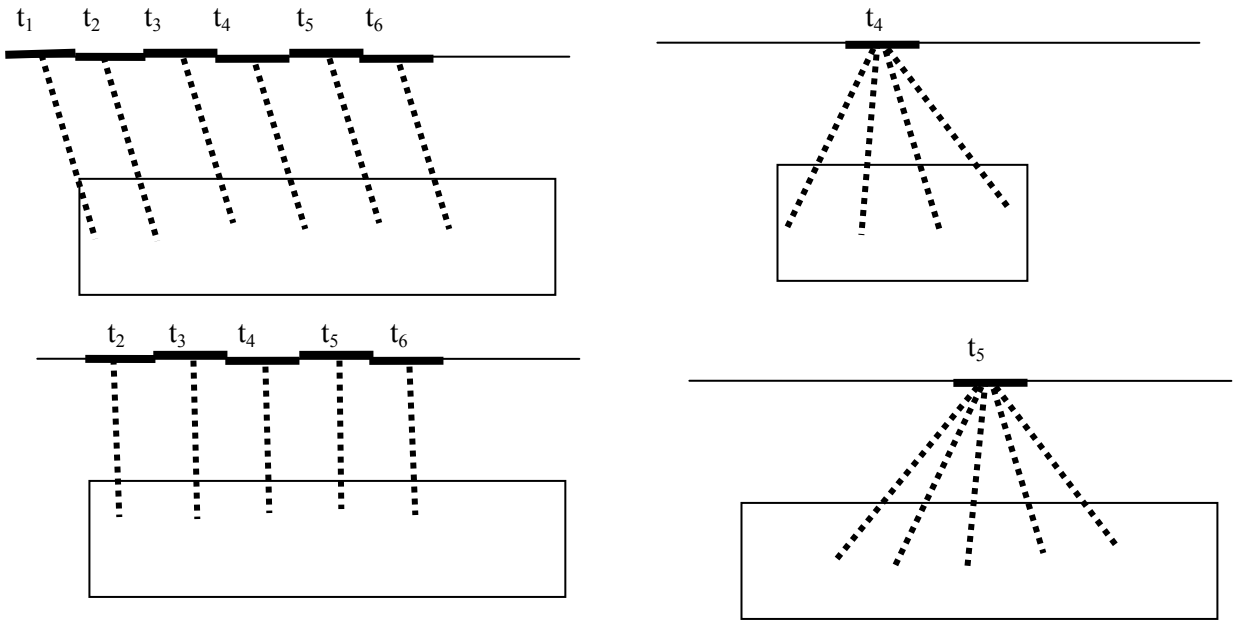


**Figure 5: Left: representation of a two stripmap images each of them processed with a constant squint angle Right: representation of two images each of them processed with varying squint angle.**

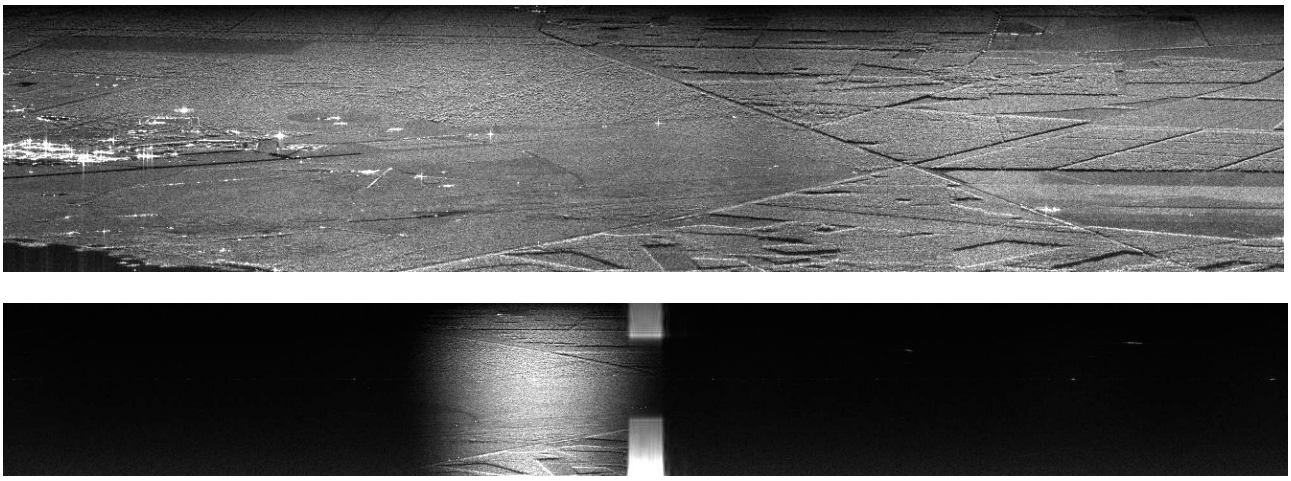

**Figure 6: Above Example of a Stripmap image. Below: example of a FDBS image. The black area corresponds to exoclutter area; the white area is due to the presence of a jammer.**

## 3.2 moving target modelling

When an object is moving on the ground the basic hypothesis of stationary targets does not hold anymore and the phase compensation as presented in equation (2) is not efficient to focus the target. Adapted SAR processing is possible knowing the movement parameters (speed, acceleration...) of the target but in general these parameters are not known so work has to be done to estimate these parameters while imaging the target [6].

### 3.2.1 Phase history

The Taylor's expansion of $R_i$ in presence of a moving target P seen from $S_1$ under a squint angle θ, with velocity vector **v** and constant acceleration vector **a** gives:

$$R_i = S_i P_i = \left|\mathbf{S_1P_1} + \mathbf{P_1P_i} - \mathbf{S_1S_i}\right| = \left|\mathbf{S_1P_1} + \mathbf{vt} + \frac{1}{2}\mathbf{a}t^2 - \mathbf{V}_s t\right| \tag{7}$$

$$R_i \approx R_1\left(1 + \frac{v_r - V_S \sin\theta}{R_1}t + \left(\frac{a_r}{2R_1} + \frac{\left|\mathbf{v} - \mathbf{V}_s\right|^2}{2R_1^2} - \frac{(v_r - V_S \sin\theta)^2}{2R_1^2}\right)t^2\right) \tag{8}$$

$v_r$ being the projection of the target velocity on the line of sight defined as the vector $S_1P_1$

Up to the first order, this target P is at the same distance from the sensor trajectory as a stationary target Q, seen from $S_1$ under the squint angle θ' such as:

$$\frac{v_r - V_S \sin\theta}{R_1} = \frac{-V_S \sin\theta'}{R_1} \text{ so}$$

$$\sin\theta' = \sin\theta - \frac{v}{V_S} \tag{9}$$

$$R_i \approx R_1\left(1 - \frac{V_S \sin\theta'}{R_1}t + \frac{V_S^2 \cos^2\theta'}{2R_1^2}t^2 + \left(\frac{a_r}{2R_1} + \frac{(v^2 - 2v_a V_S)}{2R_1^2}\right)t^2\right) \tag{10}$$

The only difference is that the FM rate is different from the FM rate of the stationary target.

Therefore, the moving target will appear on the SAR image at the squint angle of a stationary target defined in equation (9). This difference of squint angles leads to a delocalisation effect, proportional to the radial velocity of the moving target.

Furthermore, the FM rate of a moving target differs from the stationary target's one so the focusing is not efficient and the target appears defocused. The defocusing parameter is related to the FM rate error:

$$\Delta FM = -\frac{2a_r}{\lambda} - \frac{2(v^2 - 2v_a V_S)}{\lambda R_1} \tag{11}$$

It depends on both the radial acceleration and along-track velocity of the target.

0 gives some example of delocalised or defocused targets. The airplane was flying along a circular trajectory [7] and the car was moving on the road indicated by a red arrow. Depending on the orientation of the road related to the trajectory, the car is delocalised, defocused or both. In one case (image C), it cannot be distinguished from the clutter while its shadow is seen on the road.

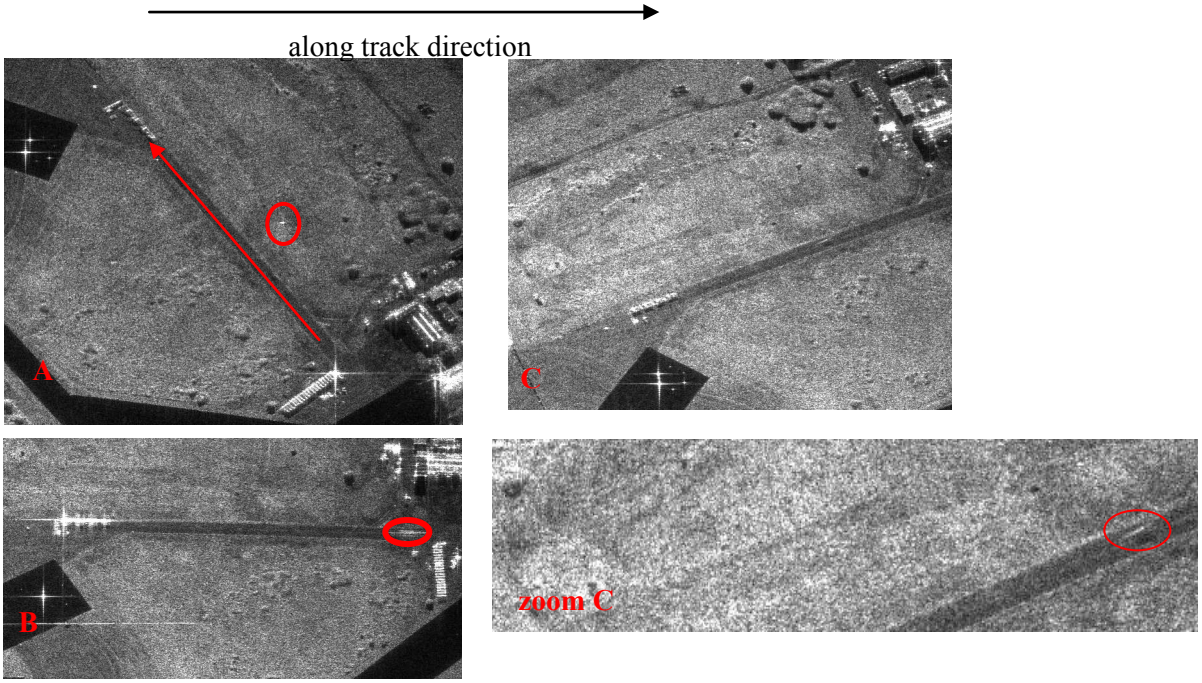


**Figure 7: SAR Images the moving target with different configurations. The red arrow gives the direction of the vehicle on the road, the red circles indicate the apparent position of the targets; in image C, the target is delocalised but cannot be seen; its shadow on the road is visible (zoom).**

### 3.2.2 Delocalisation

As explained in the last section, a moving target is delocalised: it appears at the same range as its real position but at a different squint angle.

As stripmap images are focused for a given squint angle, moving targets appear on the image at the time when its squint angle, compensated by its radial velocity is equal to the processed squint angle. The same target would appear at a different time if processed with a different squint angle.

This can also be explained geometrically as illustrated on 0: If a target is moving in the radial direction, the intersection of the corresponding iso-range circles through the integration time is located at different squint angle than the target squint angle.

Furthermore, SAR images are generally processed for the squint angle corresponding to the squint of the maximum of the antenna pattern and generally the processed bandwidth is close to the antenna pattern diagram. A moving pattern which appears in the stripmap image has been imaged at another squint angle so it has been imaged through another part of the antenna pattern and presents an amplitude modulation different from the amplitude modulation of the clutter. 0 illustrates this idea:

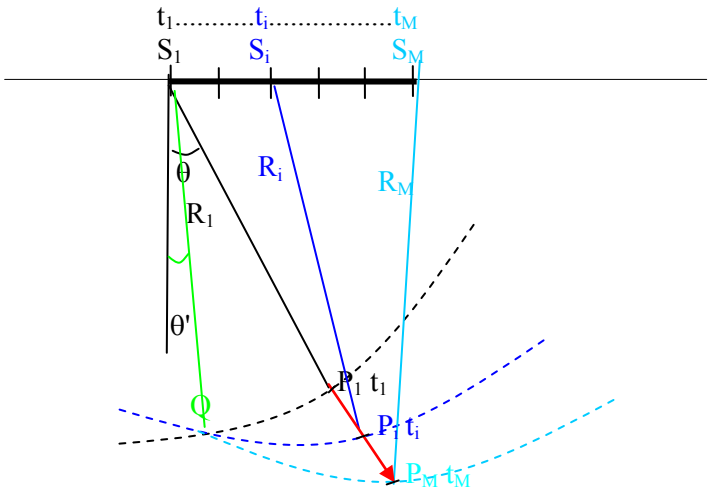


**Figure 8: Geometrical interpretation of the delocalisation effect.**

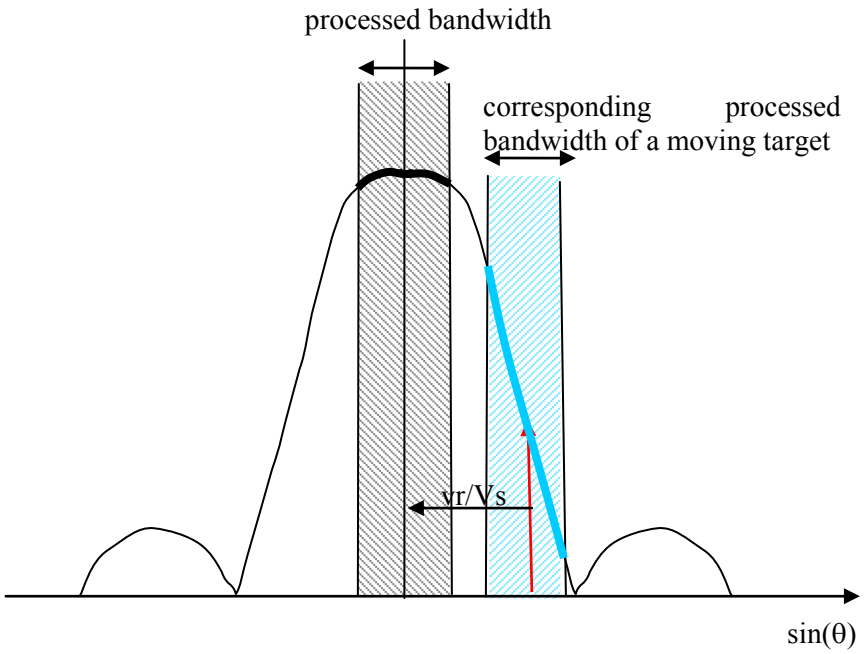


**Figure 10: Antenna pattern, processed bandwidths and delocalised target (red arrow). The amplitude modulation due to the antenna pattern on the clutter is represented in bold black, whereas the amplitude modulation due to the antenna pattern on the target is in bold blue.**

In the FDBS geometry, all the pixels of the image correspond to the same integration time. A moving target with radial velocity appears in a wrong azimuth position - in this case, each azimuth corresponds to a squint angle. This kind of image gives a snapshot of all the moving targets present at a certain time. Like in stripmap mode, supposing isotropic targets, there is an amplitude modulation of the moving target which is equal to the amplitude modulation of the clutter located at the true position of the moving target.

### 3.3.3 Defocusing

Equation (11) gives the difference of doppler frequency modulation rates between a moving target and the FM rate used for focusing the ground area which appear at the same position of the moving target on the SAR image. This defocusing effect is related to the radial acceleration of the target as well as to the along-track velocity of the target (generally $v$ is small compared to $V_S$ so the $v^2$ is negligible in equation (11)).

S. Hinz [8] gives a relationship between the length of the defocused target and its along track velocity in case of constant velocity.

$$L = 2v_a T = \frac{v_a \lambda R}{V_S res_{az} \cos^2 \theta} \tag{12}$$

## 4.0 MOVING TARGET DETECTION ON ONE IMAGE

The main issue of moving target detection is the defocusing effect which degrades the SCR (Signal to Clutter Ratio) of the target. Depending on the defocused length, the target may be completely hidden by the surrounding clutter (see 0). Moving target detection is therefore more difficult than stationary target detection.

Researchers have proposed several methods to detect moving targets and re-localise them using one single receiving antenna. We will present the three main techniques: change detection techniques, refocusing methods and re-localisation using the analysis of the amplitude modulation of the target.

### 4.1 Change detection

The idea of this method is to divide the SAR image into two azimuthal sub-band images and to use change detection techniques to follow the position of the target on the two images. Since the two sub-bands correspond to different acquisition times, the target moved from one position to the other. This technique has been proposed by M Kirscht [9] and was further developed by D. Pastina [10]. It is interesting to notice that, for the main apparent movement of the target is only in the along-track direction. 0 gives an explanation of this phenomenon: the delocalisation effect does not change with the sub-band but the defocusing effect changes.

Moving targets have the same SCR on the change detection map as on the full resolution image but they exhibit a peculiar pattern (first a target removal followed by a target appearance in the azimuth direction). This pattern is used to decrease the number of false alarms. Note that stationary non isotropic targets may have the same behaviour as moving targets since the RCS of one sub-band may be different from the other.

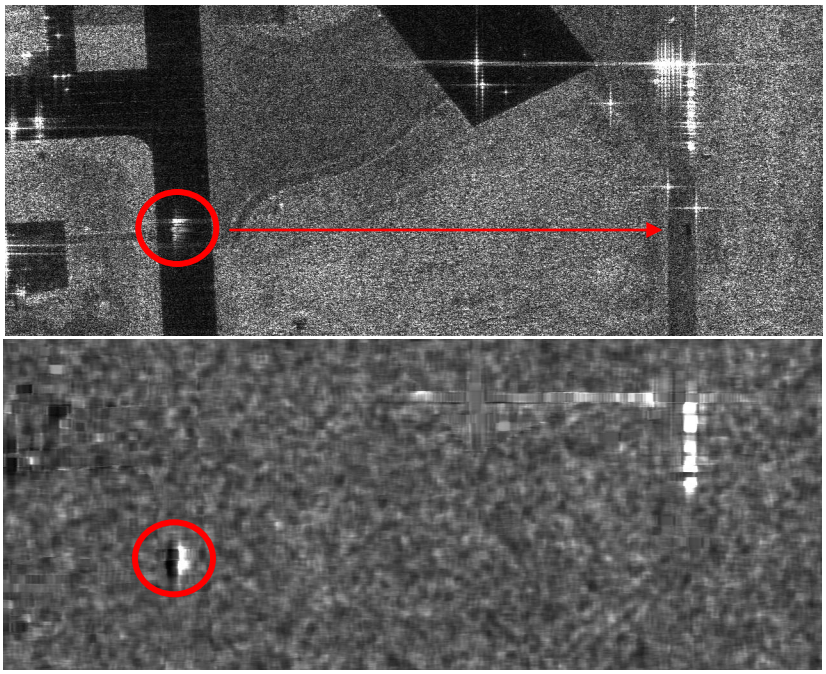

**Figure 11: Above: Image of a delocalised moving target. Below change detection result: the black area corresponds to the removal of the target and the white position to the appearance.**

## 4.2 Refocusing techniques

In order to better detect moving targets, several authors propose to refocus moving targets for different azimuthal velocities. The refocusing step may be done, by correcting the residual phase of the azimuthal Fourier transform of the moving target. Other refocusing algorithms can cope with larger bandwidth signals. They are based either on the ω-k algorithm [11] or on CSA algorithm [12]. These corrections are not adapted to the surrounding stationary clutter so, while the moving target is refocused the clutter is smeared.

0 presents the case of a high RCS target [7]. The unfocused target is displayed in A. The plot represents the unwrapped phase of the azimuthal fourier transform of the target (black) and the proposed correction. The refocused target is in B. One can notice that the surrounding clutter is blurred. Another example of a very high resolution image is presented in 0.

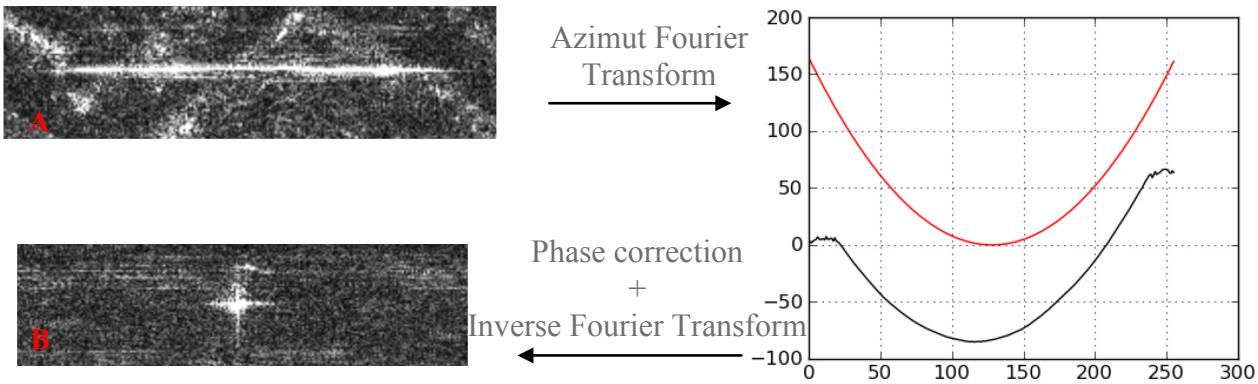


**Figure 12: Defocusing effect on a moving target.**

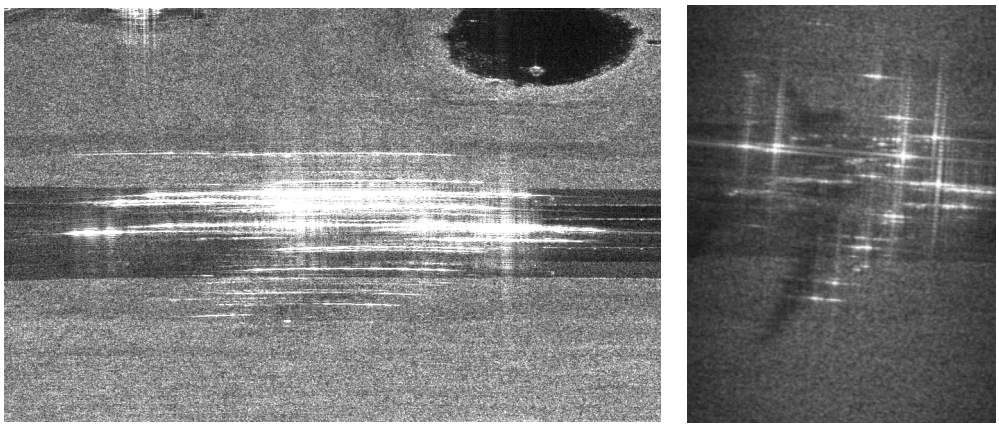

**Figure 13: Defocused airplane on a taxi-way and its refocused image (estimated velocity: 36 km/h).**

Depending on the manoeuvrability of the target and on the integration time, the second order model (equation (10)) can be not sufficient. In fact, a moving target is composed of several reflectors which may have different velocities. Furthermore, for airborne acquisitions with long integration times, the model of a constant velocity or constant acceleration target may not hold. R.P. Perry [13] proposes a methodology to refocus targets for high level orders and to separate the main contributors of the target in order to refocus each of them separately.

### 4.3 Amplitude modulation method

It is also possible to take advantage of the amplitude modulation of the moving target which is different from the clutter one [14]. This method is efficient for narrow beam radars with large variations of the beam pattern within the integrated angular extend. The main drawback is that the amplitude response of a car highly depends on the aspect angle so the amplitude modulation observed on the Doppler Fourier transform of the car is the product of the natural amplitude modulation of the car and of the beam.

### 4.4 Combination of techniques

Different authors have used simultaneously several techniques to solve this detection problem. Dias and Marquez [14] propose to use simultaneously refocusing techniques in an ω-k framework and amplitude modulation to estimate the velocity vector of the target. As stated in [14] good detection and trajectory estimation are obtained when the "moving target spectra are not totally overlapped with the clutter spectrum. Otherwise the detector and the estimator still work provided that, roughly, SCR>10dB."

Finally D. Henke [15] takes advantage of a large beam antenna to process sub-band images, to detect abnormal pixel behaviours corresponding to moving targets in the stack of images and to track these anomalies.

## 5. TWO IMAGES DETECTION

The problem of delocalisation can be solved when using more than one receiver antenna. The use of two receiving antennas aligned in the along-track direction has been thoroughly studied for low motion estimation such as currents estimation [16]. The main idea is that, using two antennas; the imaged terrain is

seen under exactly the same line of sight at two different instants. Therefore the only difference between the two acquisitions is those related to moving phenomena such as current or moving targets. The phase difference of the two resulting SAR images is therefore proportional to the radial distance travelled by the moving target between these two instants [17].

We have:

$$\varphi_{ATI} = \frac{2\pi}{\lambda} v_r \frac{d}{V_S} \tag{13}$$

with $d$ being the distance between the two receiving antennas.

This configuration gives a velocity ambiguity due to the wrapping of the interferometric phase which is equal to:

$$v_{r-amb} = \frac{\lambda V_s}{d} \tag{14}$$

These two relationships show that in order to have precise results on the velocity estimation of the target, one has to increase $d$ at the cost of a smaller velocity ambiguity.

## 5.1 Stripmap mode ATI

An example of an ATI image is presented in 0. The moving target is almost not visible in the two amplitude image of the ATI couple whereas it can be detected in the coherence image (loss of coherence image) and in the ATI phase image (ATI phase different from its surrounding). On this example, the ATI phase varies from point to point in the target signature. This is due to the superimposition of clutter and target in a same resolution cell. Let's call $s^2$, the mean RCS of the target, $\varphi$ its ATI phase, $c^2$ the mean clutter level, with a 0 ATI phase, and $n^2$ the noise level. It can be shown that:

$$coh. = \left| \frac{s^2 e^{j\varphi} + c^2}{s^2 + c^2 + n^2} \right|$$

$$\varphi_{\text{target+clutter}} = \angle(s^2 e^{j\varphi} + c^2)$$

The coherence loss depends on both the SCR of the target and its velocity. For low SCR targets, it is not possible to estimate accurately their velocity since the measure is very noisy due to coherence loss.

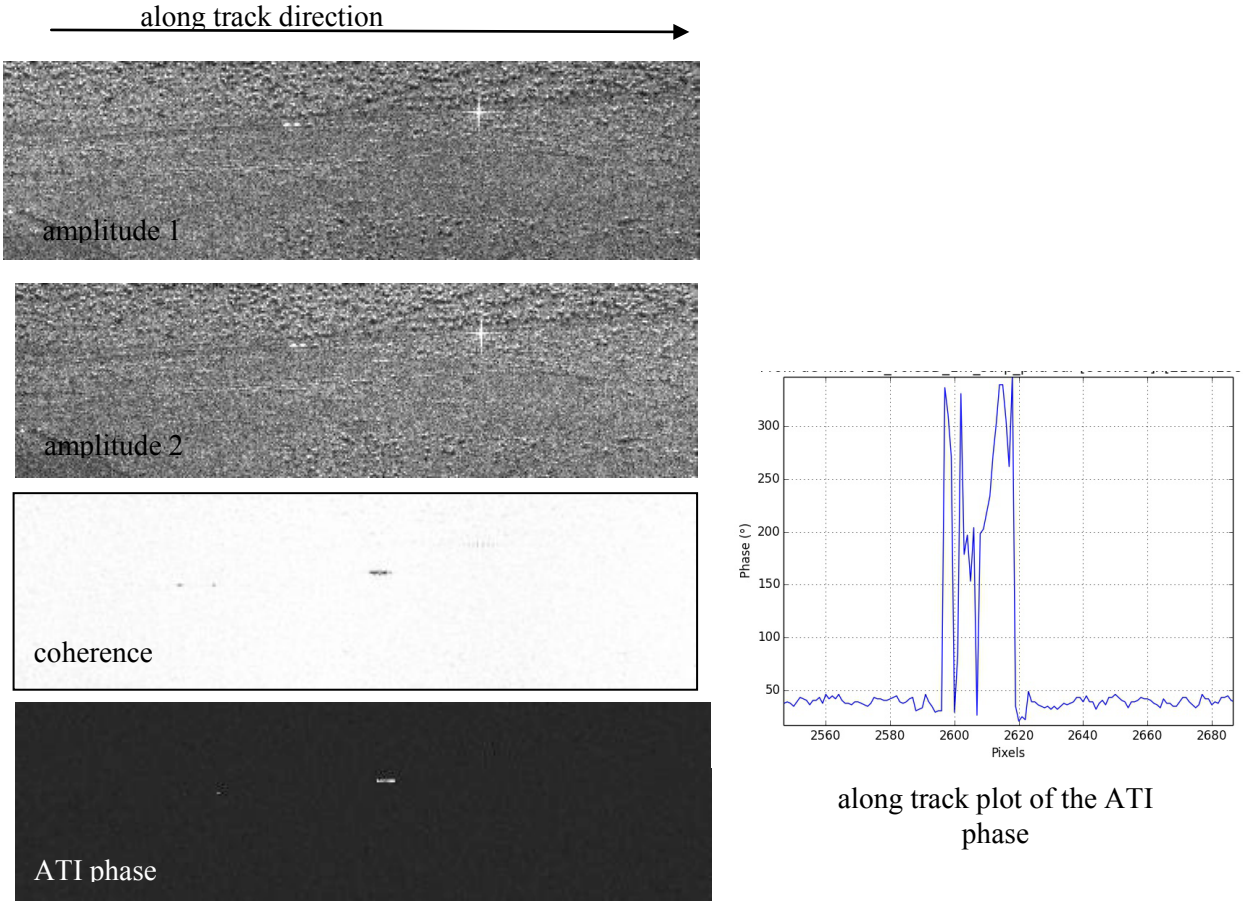


**Figure 14: The two amplitude images, coherence and ATI phase of a moving target.**

Several authors have developed CFAR detectors based on thresholding the ATI image and amplitude information [18], [8].

## 5.2 ATI in FDBS geometry

ATI can also be implemented for FDBS images (see 0)

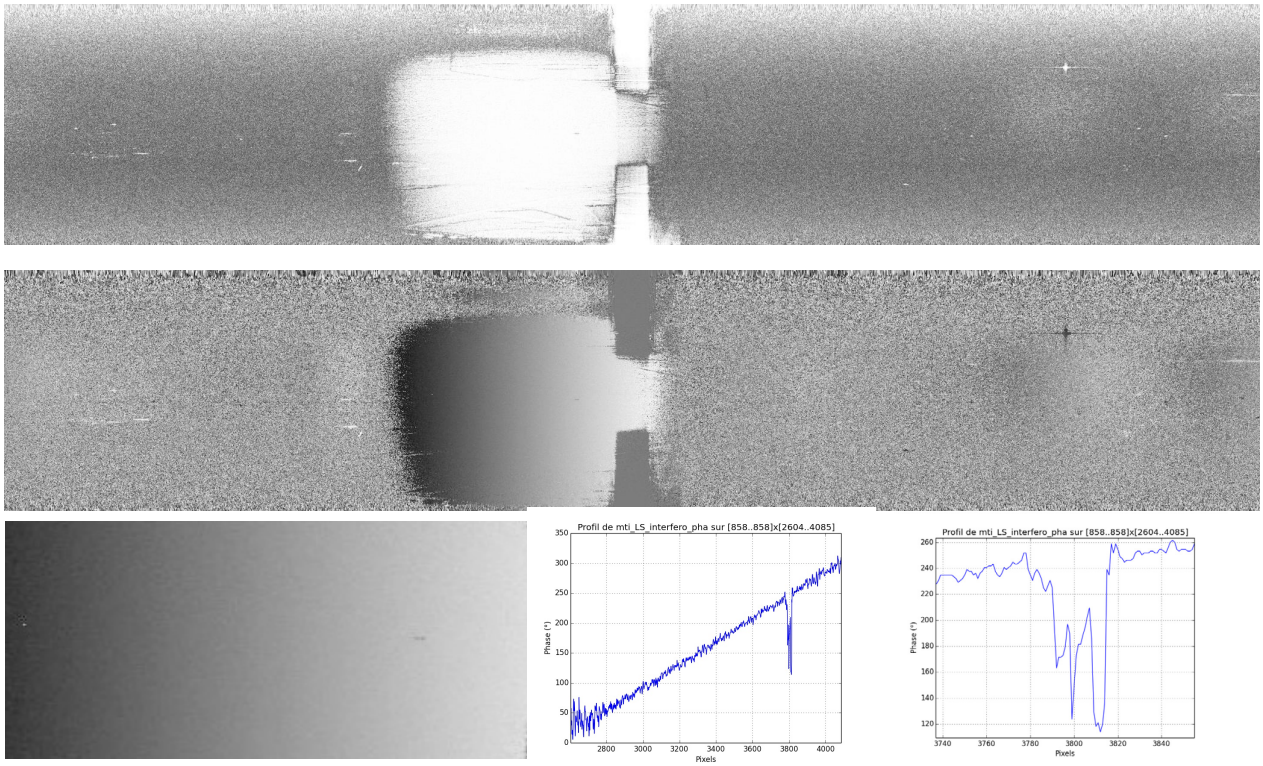


**Figure 15: FDBS mode ATI Coherence (above), ATI phase image (middle). Below: zoom of the ATI phase in the main lobe area (left), cut of the ATI phase in azimuth in presence of a target (middle) and zoom of the ATI phase of the target (right).**

The ATI interferogram in the FDBS geometry presents a linear variation in the main lobe. This variation is due to the delay difference between the two phase centres of the antennas and the imaged point.

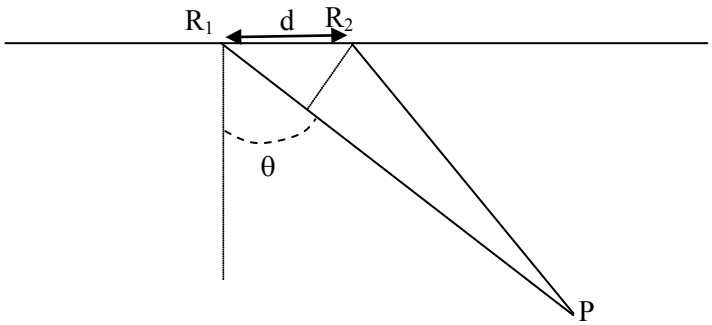


**Figure 16: ATI geometric configuration.**

$$\varphi_{ATI-FDBS} = \frac{2\pi}{\lambda} d \sin(\theta) \tag{15}$$

This phase varies with the squint angle, and therefore with azimuth. This linear variation of the ATI phase is a way to precisely calibrate *d*, the ATI baseline. Moving targets are visible since their ATI phase corresponds to the ATI phase of their true position which is different from the ATI phase of their surrounding clutter near the apparent position (see 0 below). Like in stripmap mode ATI, the FDBS ATI phase is corrupted by the clutter phase when the clutter level cannot be neglected in front of the target level.

Notice that the ATI method uses only two channels and present the same problem as STAP methods with 2 spatial channels: targets can be detected but not localised accurately.

# 6. MULTI -IMAGE TARGET DETECTION (M-SAR)

Several authors have worked on moving target detection using antennas with several receiving channels (M-SAR) unifying the STAP approach, that was first developed for non focused images, and SAR focusing. In [19], J. Ender gives the principle of such methods. These techniques have been exploited either for airborne SAR acquisitions or, more recently, for spaceborne SAR using Radarsat-2 images for instance.

Different strategies are being explored. Each of these methods proposes to use the vector composed of the M spatial channels as variable, to estimates the covariance matrix associated to this vector and perform clutter cancellation either before focusing in the range Doppler domain or after focusing.

## 6.1- STAP is performed before SAR focusing

D. Cristallini [20] proposes to cancel the clutter by working in the range-Doppler domain of the range compressed data.

The M channel signals (in the range -Doppler domain) are used to form a M by 1 signal vector **X**. The covariance matrix of the clutter is computed using secondary data for adjacent range bin and the same Doppler frequency of the signal vector. The whitened output signal is therefore:

$$X_{stap}(r, f_d) = (R^{-1}(f,d).S(f))^H X(r, fd) \tag{16}$$

With **S** being the vector taking into account the temporal delays between the M channels.

This temporal delay has to be known very precisely in order to have an efficient clutter cancellation.

A bank of SAR focusing filters corresponding to different target velocity hypotheses are then used to estimate the along-track velocity of targets. The along-track velocity of each pixel is chosen as the one maximising the filter output.

## 6.2- STAP is performed while SAR focusing

Here [21] the covariance matrix of the M channels is estimated in the Fourier domain, and the STAP test is computed in this domain: the detection is then applied after azimuth compression of the data: Schematically, clutter cancellation is computed in the range-Doppler domain while focusing the data with different velocity vectors. The detection test is applied after focusing.

$$T_{istap} = \max_{\mathrm{v}}\left(\frac{\left|\int h(f_d,\mathrm{V})\mathbf{d}^{\mathrm{H}}(f_{d,}\mathrm{V})\mathbf{R}^{-1}(d_d)X(r,f_d)e^{2\pi f_d T}df_d\right|^2}{\left|\int \mathbf{d}^{\mathrm{H}}(f_{d,}\mathrm{V})\mathbf{R}^{-1}(d_d)\mathbf{d}^{\mathrm{H}}(f_{d,}\mathrm{V})df_d\right|}\right. \tag{17}$$

h(fd,V) is the compression azimuth filter adapted to the velocity vector **V** and **d** corresponds to the steering vector of the target.

This criterion is computationally expensive since the SAR focusing is applied for different along-track and radial velocities. Sub-optimal processing schemes are proposed. Note that this formulation can deal with the azimuth ambiguity observed on satellite SAR data.

### 6.3 STAP is performed after SAR focusing in a stripmap mode

D. Cerutti [22] proposes also to (1) compress the SAR data for different velocities and for each velocity hypothesis to perform a post doppler STAP which is defined as:

$$T_{EDPCA}(i,j) = \max_{V}\left(\frac{\left|\mathbf{d}^{H}(V)\mathbf{R}^{-1}(V)X(i,j,V)\right|^{2}}{\left\|\mathbf{d}^{H}(V)\mathbf{R}^{-1}(V)X(i,j,V)\right\|}\right)$$

with d being the steering vector of the target that can take into account ambiguity targets, X is the focused signal under the velocity hypothesis **V** and R is the covariance matrix estimated on the focused images around pixel (i,j).

### 6.4 STAP is performed after SAR focusing in the FDBS

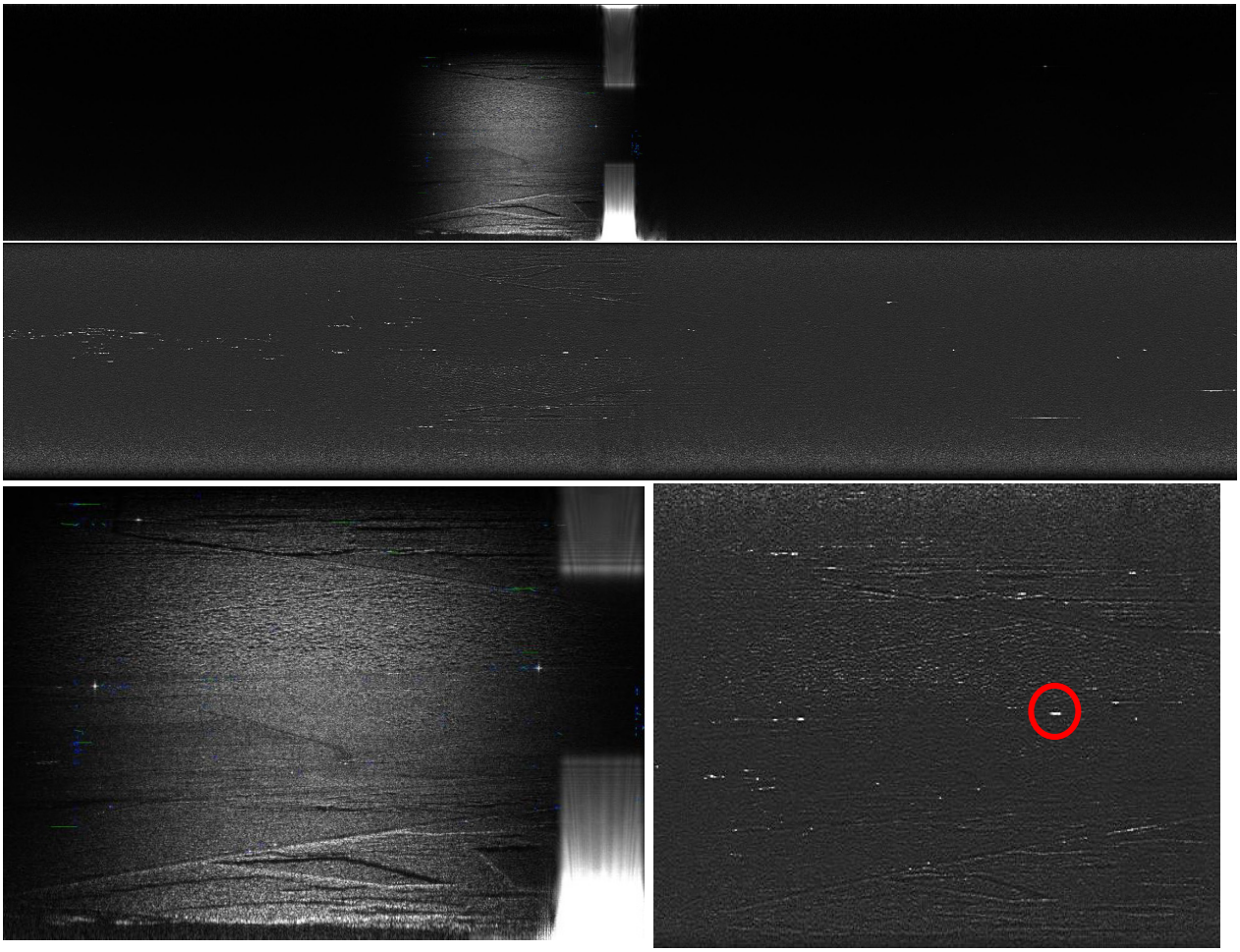

**Figure 17: Above: One channel image. Middle: STAP detection map. Below: zoom on the 2 images.**

It has also been proposed to use the FDBS geometry to detect moving targets [23], [24] using the STAP methodology. This mode does not need precise calibration since the clutter steering vector is measured directly on the images. The M channels are focused via in a FDBS configuration then STAP is applied using only the M channels. The covariance matrix is estimated on the focused images and the target detection is performed before refocusing in azimuth.

0 presents a detection map obtained using this method for a 4 receiving antenna system in X band. The jammer has been removed and the clutter has been suppressed quite efficiently. Moving targets are visible in the detection map as well as residual from high RCS stationary points.

## 7.0 CONLUSION

In this paper we presented the principles of SAR imaging techniques as well as the signatures of moving target on such images. The principle of different methods of moving targets detection and localisation have been presented from the less demanding methods in term of acquisition (one receiving channel) to the most demanding acquisition systems (M-SAR).

## 8.0 ACKNOWLEDGMENTS

The author wishes to thank the SETHI team for acquiring most of the data presented in this paper and to H. Cantalloube, L Savy and B. Vaizan for fruitful discussions on the comparison of the MTI/STAP mode with SAR.

## 9.0 REFERENCES

[1] R. Klemm, "Space-Time Adaptive Processing, principle and applications″, IEE Radar, Sonar, navigation and Avionics 9, 1998

[2] I. G. Cumming, F.H. Wong, "Digital processing of Synthetic Aperture Radar data, Algorithms and Implementation", Artech House, 2005.

[3] http://www.eupisa.school2014.iet.unipi.it/EURASIP_VIGNAUD_PISA_SEP_2014.pdf

[4] Y. Hawa, "A Study of Fast Backprojection Algorithm for UWB SAR and a Comparison between Fast- and Global Backprojection", PhD Thesis, School of Signal Processing -Blekinge Institute of Technology, Sweden,

[5] Cantalloube, H.M.J.; Nahum, C.E., "Airborne SAR-Efficient Signal Processing for Very High Resolution," *Proceedings of the IEEE* , vol.101, no.3, pp.784,797, March 2013

[6] R. Raney, "Synthetic aperture imaging radar and moving targets", *IEEE Transactions on Aerospace and Electronic Systems*, vol. AES-7, pp.499 -505 1971

[7] Poisson, J.B.; Oriot, H.M.; Tupin, F., "Ground Moving Target Trajectory Reconstruction in Single-Channel Circular SAR," *Geoscience and Remote Sensing, IEEE Transactions on* , vol.53, no.4, pp.1976,1984, April 2015

[8] Hinz, S.; Meyer, F.; Laika, A.; Bamler, R., "Spaceborne Traffic Monitoring with Dual Channel Synthetic Aperture Radar Theory and Experiments," *Computer Vision and Pattern Recognition - Workshops, 2005. CVPR Workshops. IEEE Computer Society Conference on* , vol., no., pp.7,7, 25-25 June 2005

[9] Kirscht, M., "Detection and imaging of arbitrarily moving targets with single-channel SAR," *RADAR 2002* , vol., no., pp.280,285, 15-17 Oct. 2002

[10] Pastina, D.; Battistello, Giulia; Battistello, Giulia; Aprile, Angelo, "Change detection based GMTI on single channel SAR images," *Synthetic Aperture Radar (EUSAR), 2008 7th European Conference on* , vol., no., pp.1,4, 2-5 June 2008

[11] Jen King Jao, "SAR image processing for moving target focusing," *Radar Conference, 2001. Proceedings of the 2001 IEEE* , vol., no., pp.58,63, 2001

[12] Cristallini, D.; Pastina, D.; Colone, F.; Lombardo, P., "Efficient Detection and Imaging of Moving Targets in SAR Images Based on Chirp Scaling," *Geoscience and Remote Sensing, IEEE Transactions on* , vol.51, no.4, pp.2403,2416, April 2013

[13] Perry, R.P.; DiPietro, R.C.; Fante, R., "SAR imaging of moving targets," *Aerospace and Electronic Systems, IEEE Transactions on* , vol.35, no.1, pp.188,200, Jan 1999

[14] Dias, J.M.B.; Marques, P.A.C., "Multiple moving target detection and trajectory estimation using a single SAR sensor," *Aerospace and Electronic Systems, IEEE Trans. on* , vol.39, no.2, pp.604,624, April 2003

[15] Henke, D.; Magnard, C.; Frioud, M.; Small, D.; Meier, E.; Schaepman, M.E., "Moving-Target Tracking in Single-Channel Wide-Beam SAR," *Geoscience and Remote Sensing, IEEE Transactions on* , vol.50, no.11, pp.4735,4747, Nov. 2012

[16] R. M. Goldstein and H. A. Zebker, "Interferometric radar measurement of ocean surface currents", *Nature*, vol. 328, no. 6132, pp.707 -709 1987

[17] Suchandt, S.; Palubinskas, G.; Scheiber, R.; Meyer, F.; Runge, H.; Reinartz, P.; Horn, R., "Results from an airborne SAR GMTI experiment supporting TerraSAR-X traffic processor development," *Geoscience and Remote Sensing Symposium, 2005. IGARSS '05. Proceedings. 2005 IEEE International* , vol.4, no., pp.2949,2952, 25-29 July 2005

[18] Gierull, C.H., "Statistical analysis of multilook SAR interferograms for CFAR detection of ground moving targets," *Geoscience and Remote Sensing, IEEE Trans. on* , vol.42, no.4, pp.691,701, April 2004

[19] Ender, J.H.G., "Space-time adaptive processing for synthetic aperture radar," *Space-Time Adaptive Processing (Ref. No. 1998/241), IEE Colloquium on* , vol., no., pp.6/1,618, 6 Apr 1998

[20] Cristallini, D.; Colone, F.; Pastina, D.; Lombardo, P., "Integrated clutter cancellation and high-resolution imaging of moving targets in Multi-channel SAR," *Radar Conference, 2009. EuRAD 2009. European* , vol., no., pp.57,60, Sept. 30 2009-Oct. 2 2009

[21] Cerutti-Maori, D.; Sikaneta, I.; Gierull, C.H., "Optimum SAR/GMTI Processing and Its Application to the Radar Satellite RADARSAT-2 for Traffic Monitoring," *Geoscience and Remote Sensing, IEEE Transactions on* , vol.50, no.10, pp.3868,3881, Oct. 2012

[22] Cerutti-Maori, D.; Sikaneta, I., "A Generalization of DPCA Processing for Multichannel SAR/GMTI Radars," *Geoscience and Remote Sensing, IEEE Transactions on* , vol.51, no.1, pp.560,572, Jan. 2013

[23] H. Cantalloube, "Mobile Target Indication from Focused Flashlight SAR Images", *Proceedings of EUSAR 2004*.

[24] H. Oriot, B. Vaizan, "Preliminary results on Ground Moving Target Detection with L band data acquired with the RAMSES sensor", *Proceedings of EUSAR*, Dresden, Germany, May 2006.